Effect of MWCNT functionalization on thermal and electrical properties of PHBV/MWCNT nanocomposites

Thaís Larissa do Amaral Montanheiro[a)] and Fernando Henrique Cristóvan
Universidade Federal de São Paulo (UNIFESP), Instituto de Ciência e Tecnologia, São José dos Campos, São Paulo 12.231-280, Brazil

João Paulo Barros Machado
Instituto Nacional de Pesquisas Espaciais (INPE), Laboratório Associado de Sensores e Materiais (LAS), São José dos Campos, São Paulo 12.245-970, Brazil

Dayane Batista Tada
Universidade Federal de São Paulo (UNIFESP), Instituto de Ciência e Tecnologia, São José dos Campos, São Paulo 12.231-280, Brazil

Nelson Durán
Universidade Estadual de Campinas (UNICAMP), Instituto de Química, Campinas,São Paulo 13.083-970, Brazil; and Universidade Estadual de Campinas (UNICAMP), Laboratory on Nanostructures Synthesis and Biological Interactions (NanoBioss), Campinas, São Paulo 13.083-970, Brazil

Ana Paula Lemes
Universidade Federal de São Paulo (UNIFESP), Instituto de Ciência e Tecnologia, São José dos Campos, São Paulo 12.231-280, Brazil; and Universidade Estadual de Campinas (UNICAMP), Instituto de Química, Campinas, São Paulo 13.083-970, Brazil

Pristine multiwalled carbon nanotubes (P-MWCNTs) were functionalized with carboxylic groups (MWCNT-COOH) through oxidation reactions and then reduced to produce hydroxyl groups (MWCNT-OH). Pristine and functionalized MWCNTs were used to produce poly (hydroxybutyrate-co-hydroxyvalerate) (PHBV) nanocomposites with 0.5 wt% of MWCNTs. MWCNT functionalization was verified by visual stability in water, infrared and Raman spectroscopy, and zeta potential measurements. Pristine and functionalized MWCNTs acted as the nucleating agent in a PHBV matrix, as verified by differential scanning calorimetry (DSC). However, the dispersion of filler into the matrix, thermal stability, and direct current (DC) conductivity were affected by MWCNT functionalization. Scanning electron microscopy (SEM) showed that filler dispersion into the PHBV matrix was improved with MWCNT functionalization. The surface roughness was reduced with the addition and functionalization of MWCNT. The thermal stability of PHBV/MWCNT-COOH, PHBV/P-MWCNT, and PHBV/MWCNT-OH nanocomposites were 20, 30, and 30 °C higher than neat PHBV, respectively, as verified by thermogravimetry analysis (TGA). Addition of pristine and functionalized MWCNTs provided electrical conductivity in nanocomposite, which was higher for PHBV/P-MWCNTs (1.2×10^{-5} S cm^{-1}).

I. INTRODUCTION

In the last two decades, biodegradable polymers have received special attention.[1] The dependence on petroleum resources can be minimized by the development of bioplastics, which can be obtained from biological and fossil resources or combinations of both.[2]

With correct disposal and composting, the pollution caused by nondegradable plastics can be controlled with the use of bioplastics.[3] For this purpose, polyhydroxyalkanoates (PHAs) are very promising alternatives, due to their biodegradability.[4] This class of biopolymer is produced by a wide diversity of microorganisms as intracellular carbon and energy storage.[5,6]

PHAs can be decomposed inside or outside cells of microorganisms, by hydrolysis reactions that are catalyzed by specific enzymes. During hydrolysis reactions, the molecules of water cause scission of ester bonds, producing carboxylic acid and alcohol groups.[7] In the natural environment, PHAs are decomposed to carbon dioxide and water (aerobic conditions) or methane and water (anaerobic conditions).[8]

Poly(hydroxybutyrate-co-hydroxyvalerate) (PHBV) is the most commonly synthesized polyester from the PHA family[9] but is brittle and has low impact resistance, low elongation at break, high crystallinity, and slow

crystallization rate that makes it not suitable for technical applications.[10–12] To solve these problems, the development of PHBV nanocomposites has been widely studied.

One of the most cited filler is carbon nanotube (CNT) due to its exceptional properties, such as high elastic modulus, tensile strength, fracture toughness, exceptional electrical, and thermal conductivity,[13] high chemical stability, and large specific area.[14]

One disadvantage in the use of CNT as a nanofiller to produce nanocomposites is the tendency to form bundles due to van der Waals interactions,[15] so its exceptional properties are not fully transferred to the matrix. So, covalent or noncovalent functionalization techniques are used to improve CNT dispersion on the matrix. Covalent functionalization consists in attachment of functional groups to the CNT surface, to disrupt its extended conjugation.[16] In addition, the functionalization of CNTs can be used in the development of several kinds of polymer/CNT nanocomposites, whereas the functionalization can result in great changes in the properties of CNTs.

In this work, we performed oxidation and reduction reactions on multiwalled CNTs (MWCNTs) and used pristine, oxidized and reduced MWCNTs to produce nanocomposites with PHBV. The MWCNT functionalization reactions were evaluated through visual dispersion stability, infrared and Raman spectroscopy, and zeta potential measurements. The MWCNT dispersion and adhesion to PHBV matrix were analyzed by scanning electron microscopy (SEM), the thermal stability and crystallization behaviors were verified by thermogravimetry (TGA) and differential scanning calorimetry (DSC), respectively, and the electrical conductivity of nanocomposites was also measured.

II. EXPERIMENTAL

A. Materials

Poly (3-hydroxybutyrate-co-3-hydroxyvalerate) (PHBV) was provided by PHB Industrial, São Paulo, Brazil, with 15 mol% of hydroxyvalerate units and molecular weight (M_w) of 230.000 g mol^{-1}. The material was used as received.

MWCNTs produced by chemical vapor deposition with a minimum purity of 93% (weight) were supplied by CNT CO. LTD., South Korea. The diameter range of the MWCNTs is from 10 to 40 nm and the length is from 5 to 20 μm.

B. CNT oxidation (MWCNT-COOH)

P-MWCNTs were functionalized with carboxyl groups by oxidation reactions with nitric acid (HNO$_3$). The MWCNT suspension was allowed in a solution of HNO$_3$ 3 mol L^{-1} under reflux at 120 °C for 12 h.

After the oxidation period, the sample was filtered under vacuum and washed thoroughly with distilled water.

C. CNT reduction (MWCNT-OH)

The resulting oxidized MWCNTs (MWCNT-COOH) were functionalized with hydroxyl groups using lithium aluminum hydride (LiAlH$_4$) dissolved in anhydrous tetrahydrofuran (THF) and refluxed for 12 h under N$_2$ atmosphere. The reduced MWCNT were filtered under vacuum and washed with acetone.

D. Nanocomposite preparation

Films of PHBV/P-MWCNT 0.5% (w/w), PHBV/MWCNT-COOH 0.5% (w/w), and PHBV/MWCNT-OH 0.5% (w/w) were prepared using the solution-casting method. In all cases, the PHBV mass was dissolved in chloroform. The CNTs were previously dispersed in chloroform using a Hielscher UP200S (200 W, 24 kHz; Hielscher Ultrasonics GmbH, Teltow, Brandenburg, Germany) ultrasonic processor with 35% of amplitude. The suspension of CNTs and PHBV solution were mixed, and the resulting volume was poured onto a Petri plate. The mixtures were allowed to stand overnight, and the films were formed after evaporation of chloroform.

E. Characterization of MWCNTs

To have an estimate of functionalization, MWCNTs were dispersed in water and chloroform before and after functionalization to evaluate the suspension stability. They were dispersed for 5 min in ultrasonic bath and photographed at time intervals. Infrared spectroscopy (FTIR) was performed using a Shimadzu IR Affinity-1 Spectrometer, with 2 cm^{-1} resolution to confirm the presence of functional groups on the surface of MWCNTs. The samples were prepared onto potassium bromide (KBr) crystals. Raman analysis was carried out using a Raman Renishaw 2000 spectrometer (Renishaw, Old Town, Gloucestershire, UK), coupled to an optical microscope with argon laser (514 nm). Zeta potential values were obtained by using a dynamic light scattering equipment, Beckman Coulter Delsa Nano (Beckman Coulter, Brea, CA). MWCNTs were dispersed in a potassium chloride (KCl) solution of 1 mM (pH 6), and the measurements were performed at 25 °C at an angle of 15°. To calculate the zeta potential from mobility values, the equation[17] of Smoluchowski was used, with values of refractive index, dielectric constant, and viscosity of water at 25 °C.

F. Characterization of nanocomposite films with PHBV

The fracture surface morphology of the nanocomposites was observed by SEM using a JEOL JSM 6360-LV microscope (JEOL USA Inc., Peabody, MA), operating at 20 keV with detectors of secondary electrons. The samples were covered in a MED020 Bal-tec sputter (Leica Microsystems, Wetzlar, Hessen, Germany) with Au/Pd alloy. The surface roughness was quantified

through perfilometry using a WYKO NT1100 optical profiling system (Veeco, Tucson, AZ).

The crystallization and melting behaviors of nanocomposites were characterized by DSC using a TA Instruments 2910 equipment (TA Instruments Waters LLC, New Castle, DE). Samples were sealed in an aluminum DSC pan and heated from room temperature to 200 °C at 10 °C min^{-1}. They were kept at 200 °C for 2 min to eliminate the heat history, subsequently cooled to −30 °C at 10 °C min^{-1}, and kept at this temperature during the 2 min. After this, they were heated to 200 °C at 10 °C min^{-1} under nitrogen atmosphere with a flow rate of 50 mL min^{-1}.

The % degree of crystallinity was calculated according to the relation: Xc (%) = $\Delta H_{m1}/W_{PHBV} \times \Delta H_m^0$, where ΔH_{m1} is the total melting enthalpy on second heating, W_{PHBV} is the weight fraction of PHBV in the nanocomposite, and ΔH_m^0 is the theoretical melting heat value of 100% crystalline PHBV, which was taken as 109 J g^{-1}.[18]

The thermal stability of the nanocomposites containing PHBV and CNTs before and after functionalization was evaluated by thermogravimetric analysis, using a simultaneous TGA/DSC Analyser SDT Q600 from TA Instruments. The samples were heated from room temperature to 1000 °C at a heating rate of 10 °C min^{-1}, under nitrogen atmosphere with a flow rate of 100 mL min^{-1}.

The DC conductivity of the nanocomposites was measured using a Keithley 2400 SourceMeter (Keithley Instruments, Inc., Cleveland, OH) and the usual two probe method. The measurements were performed using films with an average thickness of 40 μm. The electrical contact was gold/palladium thin film deposited by sputtering on both sides of the sample producing a metal–nanocomposite–metal structure. The electrical conductivity of the samples was calculated from the following equation:

$$\sigma = \frac{iL}{VA} \quad ,$$

where σ is the electrical conductivity (S cm^{-1}); i is the electric current (A); L is the sample thickness (cm); V is the voltage (V); and A is the electrical contact area (cm^2).

III. RESULTS AND DISCUSSION
A. Suspension stability

The suspension stability in water provides an estimation of the functionalization degree of a nanoparticle due to the fact that when a surface is subjected to functionalization reactions, functional groups are formed, and they can be positively or negatively charged. The presence of the same-sign electrostatic charges on the CNT surface makes them repel one another, maintaining the dispersed material.

The stability of CNT dispersion state is a valuable indication of its dispersion quality, as CNT tends to reaggregate into bundles with time in an unstable environment. The longer the dispersion lasts and the fewer/smaller that CNT bundles occur, the higher its dispersion quality.[19]

Here, a simple optical observation of CNT bundles was applied to evaluate dispersion quality and functionalization reactions. This approach cannot determine the absolute quality of dispersion, but it is useful for comparative studies, where the samples were compared under identical conditions.

Figure 1 shows the suspension stability in water for P-MWCNT (Flask 1), MWCNT-COOH (Flask 2), and MWCNT-OH (Flask 3), immediately after ultrasonication [Fig. 1(a)] and 24 h after ultrasonication [Fig. 1(b)], 13 days after ultrasonication [Fig. 1(c)], and 72 days after ultrasonication [Fig. 1(d)].

The stability of the P-MWCNT aqueous suspension is lower than that of functionalized MWCNTs, since they form agglomerates that settle at the bottom of the flask immediately after ultrasonication. The hydrophobicity of P-MWCNTs and their high van der Waals attractive force cause their agglomeration. Samples of MWCNT-COOH and MWCNT-OH showed better stability because of the presence of functional groups on their surface, which enhanced their hydrogen-bonding abilities, through the conversion of the MWCNT surface from a hydrophobic to hydrophilic state;[20] but, MWCNT-OH after a period of 13 days was still stable, while it was possible to observe some agglomerates on the MWCNT-COOH sample, and the reason is because hydroxyl groups are smaller than carboxyl groups, and they form hydrogen bonds easily, which keeps the nanotubes dispersed. After 72 days, MWCNT-OH still had a stable suspension, and MWCNT-COOH showed more agglomerates at the bottom of the flask. The stability in water was better for the MWCNT-OH sample, and the reason is because hydroxyl groups are smaller than carboxyl groups, and they form hydrogen bonds easily, which keeps the nanotubes dispersed.

B. Zeta potential

Zeta potential is an index of the magnitude of the electrostatic interaction between colloidal particles and has already been used to discuss the density of acidic sites on the surface of MWCNTs and their stability in colloidal systems.[17]

Zeta potential measurements were performed at pH 6, the same was used to analyze the MWCNTs stability in the aqueous systems. Table I shows the values of zeta potential for P-MWCNT, MWCNT-COOH, and MWCNT-OH samples.

The zeta potential value found for P-MWCNT is 0.75 mV. Pristine CNTs have low colloidal stability. This result is in accordance with the low dispersion stability in water mentioned before, which is a result of

low surface charges on P-MWCNT, which is insufficient in preventing agglomeration of CNTs and their precipitation in aqueous suspensions.

The oxidation and reduction reactions result in functional groups being attached to the surface of CNTs, which produces a negative net charge that is responsible for preventing agglomeration.

The zeta potential for MWCNT-COOH is −21.03 mV and for MWCNT-OH is −15.31 mV, which indicates that they are fairly stable in water. It was observed during stability tests that the colloidal stability from both samples was more stable over the days. The solutions of charged colloidal particles with such a zeta potential are believed to be stable in water according to the theory of colloid stabilization.[21]

MWCNT-COOH sample showed a zeta potential more negative than MWCNT-OH, and it may be explained because carboxylic groups deprotonate in pH 6, while hydroxyl groups do not. The MWCNT-OH sample also showed a negative potential, due to the electron cloud that makes them negatively charged. However, stability in water was better for the MWCNT-OH sample, as indicated in the suspension stability section, and as already discussed, the reason is because hydroxyl groups are smaller than carboxyl groups, and they form hydrogen bonds easily, which keeps the nanotubes dispersed.

The enlarged values of zeta potential of MWCNT-COOH and MWCNT-OH are in accordance with the much improved dispersion stability in water. The dispersion stability of pristine and functionalized CNT in water has a strong relationship with the zeta potential.

IV. INFRARED SPECTROSCOPY

Figure 2 summarizes the behavior of the functional groups observed via infrared spectroscopy of P-MWCNT, MWCNT-COOH, and MWCNT-OH samples.

The spectra indicate intensive bands at 3436 cm^{-1} (stretching vibrations of isolated surface –OH moieties and/or –OH in carboxyl groups and in sorbed water).[22] For P-MWCNT and MWCNT-COOH spectrum, asymmetric methyl stretching band at 2960 cm^{-1} and asymmetric/symmetric methylene stretching bands at 2923 and 2853 cm^{-1} are observed, respectively. It is usually assumed that these groups are located at the defect sites on the sidewall surface.[23] For MWCNT-OH,

TABLE I. Zeta potential values of P-MWCNT, MWCNT-COOH, and MWCNT-OH.

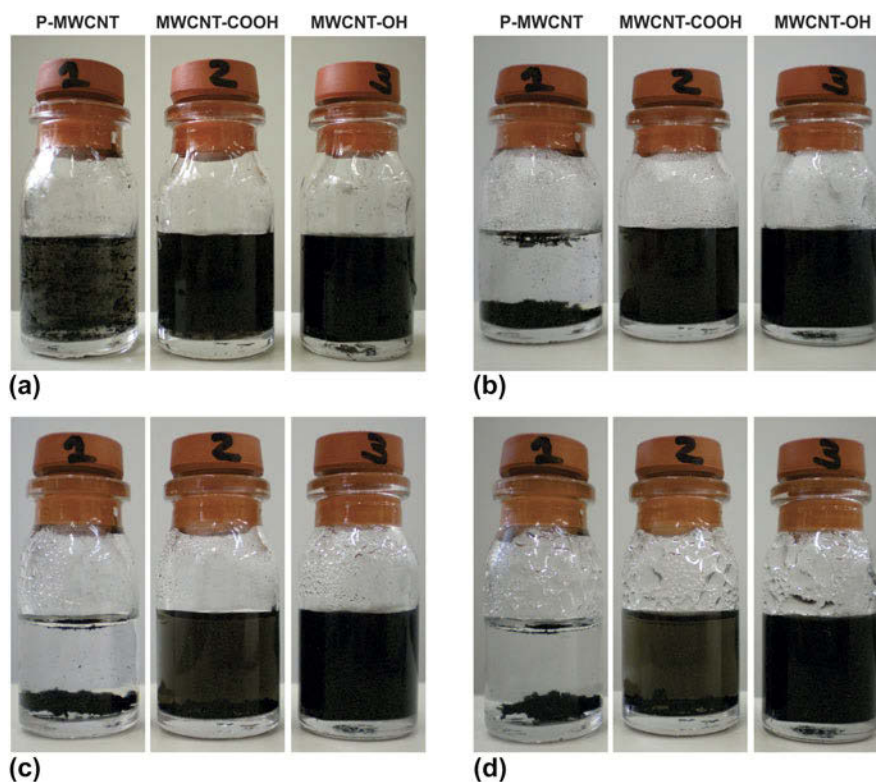| Sample	Zeta potential (mV)
P-MWCNT	0.75
MWCNT-COOH	−21.03
MWCNT-OH	−15.31

FIG. 1. Suspension stability in water for P-MWCNT (Flask 1), MWCNT-COOH (Flask 2), and MWCNT-OH (Flask 3): (a) immediately after ultrasonication, (b) 24 h after ultrasonication, (c) 13 days after ultrasonication, and (d) 72 days after ultrasonication.
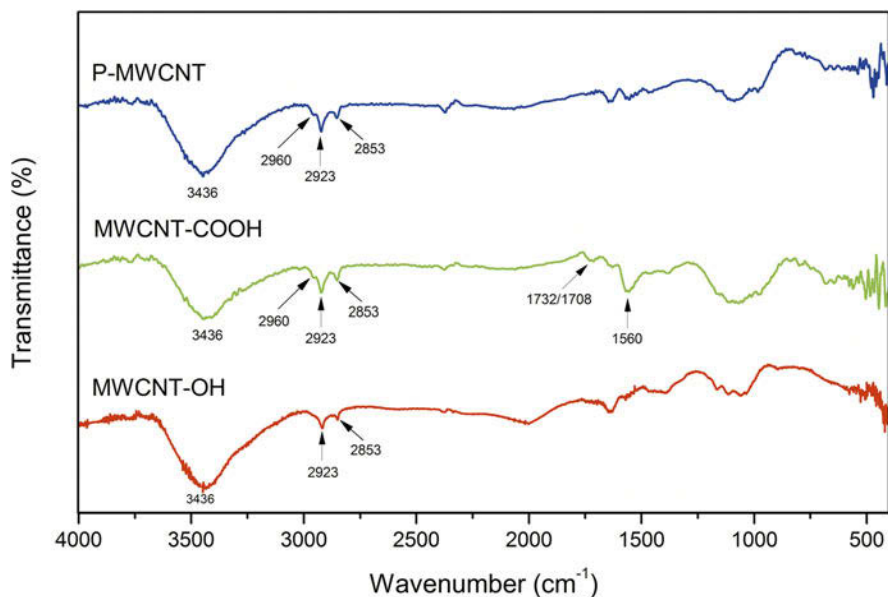
FIG. 2. FTIR spectra of P-MWCNT, MWCNT-COOH, and MWCNT-OH.

spectrum bands at 2923 and 2853 cm^{-1} decrease greatly, which implies that the alkyl chains were cleaved from the surface of the nanotubes.[24]

The C–O bands characteristic of carboxyl functional groups on MWCNT-COOH surface are observed at 1732, 1708, and 1560 cm^{-1}. The peak at 1560 cm^{-1} is related to the carboxylate anion stretch mode.[14] These bands are not seen on P-MWCNT and MWCNT-OH spectrum.

A. Raman spectroscopy

Raman spectroscopy is a technique widely used for the analysis of CNTs, because it provides information of the structure disorder degree. The Raman spectra for P-MWCNT, MWCNT-COOH, and MWCNT-OH are shown in Fig. 3, and Raman data are shown in Table II. From Fig. 3, it can be noted that all spectra are quite similar and have the same pattern, which means that the global structure of a graphene sheet does not suffer major damages during functionalization treatments.[25] This is an advantage because severe conditions of oxidation can cause great damage to the MWCNT structure and, consequently, a decrease in their reinforced action in nanocomposites. This way, it is expected that oxidation reactions create the desired functional groups while preserving the MWCNT structure as much as possible.

The spectra consist of the main G band, which is the high-frequency E_{2g} first-order mode,[26] and two disorder bands, D and D$'$. The D band is a double-resonance Raman mode, which can be understood as a measurement of structural disorder coming from amorphous carbon and any defects,[27] and D$'$ band may be assigned to the disorder-induced effect due to the finite size effect or lattice distortion.[24]

Differences in the wave number of the G and D bands can be found for other CNTs, and it is probably because of different CNT specimens, laser-illuminated positions, and incident laser power.[24] The ratio between the intensities of the G and D characteristic bands is a quantification of the functional groups introduction, by measuring the sp^3 carbon atoms introduced.[25] As lower this ratio, higher the amount of sp^3 carbon atoms; in other words, higher the amount of functional groups.

Comparing the ratio of I_G/I_D from the samples, which is 1.34 for P-MWCNT, 1.17 for MWCNT-COOH, and 1.07 for MWCNT-OH, it can be concluded that the degree of disorder is modestly improved through the functionalization reactions.

On oxidation reaction, some defects are created on the MWCNT structure related to production of carboxylic groups on the surface of CNTs. On reduction reactions, these carboxylic groups are converted into hydroxyl groups, and therefore, no new defects are created. The difference found on I_G/I_D ratios is quite small, meaning that the structure of CNTs was maintained after functionalization. The reduction observed in the I_G/I_D ratio after oxidation must be attributed to the introduction of new defects and changes in the MWCNT geometry caused by the binding of new functional groups, and after reduction, the difference in the I_G/I_D ratio must be attributed only to changes in the MWCNT geometry caused by the binding of new functional groups.[23] This is an indication that functionalization is inducing a disorder that, as a result, gives an increase in the D band area.[28]

Scheibe et al.[23] also performed oxidation and reduction reactions on MWCNTs and found that the I_G/I_D ratio is modestly reduced through reduction reaction.

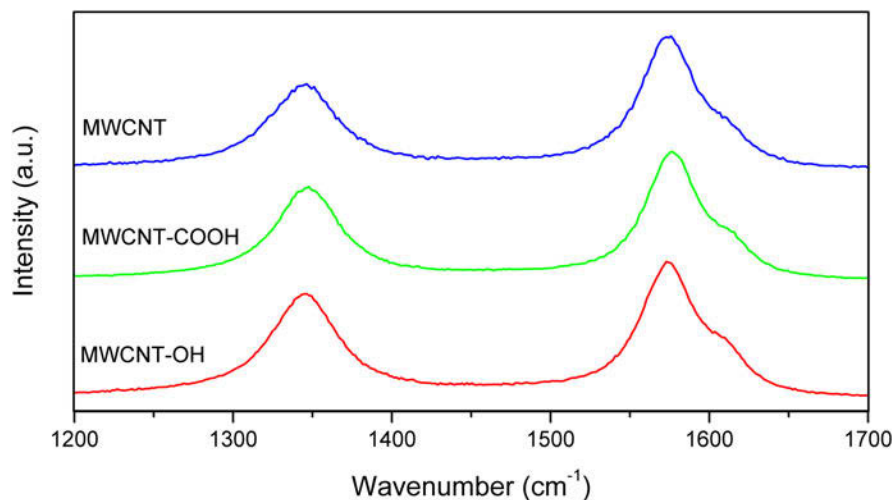J. Mater. Res., Vol. 30, No. 1, Jan 14, 2015

59

FIG. 3. Raman spectra of P-MWCNT, MWCNT-COOH, and MWCNT-OH.

TABLE II. Raman data of the characteristic peaks of P-MWCNT, MWCNT-COOH, and MWCNT-OH.

Sample	X_D, cm^{-1}	X_G, cm^{-1}	$X_{D'}$, cm^{-1}	I_G/I_D
P-MWCNT	1346.6	1573.4	1613.3	1.34
MWCNT-COOH	1344.9	1577.4	1614.9	1.17
MWCNT-OH	1345.9	1574.8	1611.9	1.07

B. Morphology

SEM images and average roughness values (Ra) of fracture surfaces of the nanocomposites are shown in Fig. 4: (a) PHBV, (b) PHBV/P-MWCNT, (c) PHBV/MWCNT-COOH, and (d) PHBV/MWCNT-OH.

The fracture surface of neat PHBV, shown on Fig. 4 (a), compared with the surface of the nanocomposites, exhibits great irregularity, with an average roughness value of 868 nm. This irregularity must be attributed to the sliding of the polymer chains, indicating that the PHBV matrix suffered great deformation during the fracture.

The fracture surface of the nanocomposite containing P-MWCNT showed some small regions with smooth surface and regions with great irregularity, in which were found lots of P-MWCNT bundles. The average roughness for the nanocomposite with P-MWCNT is 443 nm. The irregularity observed indicates that the PHBV matrix suffered a larger deformation in these regions during the fracture; however, the deformation is smaller than that for neat PHBV. It is also possible to observe a great amount of unsheltered P-MWCNTs on the surface. The fracture surface of the nanocomposites with functionalized CNTs was, mostly, smooth, as shown in Figs. 4(c) and 4(d). The average roughness for the nanocomposites with functionalized MWCNTs was decreased compared with that of neat PHBV and of the nanocomposite with P-MWCNT.

The average surface roughness for the nanocomposite with MWCNT-COOH is 289 nm and for the nanocomposite with MWCNT-OH is 297 nm.

On both cases, it is possible to observe only some fragments of unsheltered CNTs. The functional groups existing on MWCNT-COOH and MWCNT-OH surfaces reduce the van der Waals forces, reducing the strong tendency of CNTs to form bundles.

Apparently, MWCNT-COOH were better dispersed than MWCNT-OH in the PHBV matrix owing to being more embedded by the polymer and with a lower surface roughness. In Fig. 4(d), it is possible to find more fragments on unsheltered CNTs than in Fig. 4(c), indicating the existence of a better interaction of functional group COOH with PHBV matrix.

These images obtained by SEM have a very strong relationship with the zeta potential values obtained for the CNTs. Both samples of MWCNT-COOH and MWCNT-OH showed negative zeta potential values, with most negative value for MWCNT-COOH. This was directly reflected in the CNTs dispersion inside the PHBV matrix. P-MWCNT showed zeta potential value near zero, reflecting its strong tendency to form bundles, which could be easily observed.

C. Differential scanning calorimetry (DSC)

DSC analyses were performed to determine the melting and crystallization behavior for PHBV and its nanocomposites. Figure 5 shows the DSC results for neat PHBV and its nanocomposites containing pristine and functionalized CNTs. Figure 5(a) shows DSC curves for the first heating, Fig. 5(b) for cooling, and Fig. 5(c) for second heating. Table III shows the values of melting temperature (T_m), melting enthalpy (ΔH_m), degree of crystallinity (X_c), and glass transition temperature (T_g) obtained in the second heating and the crystallization
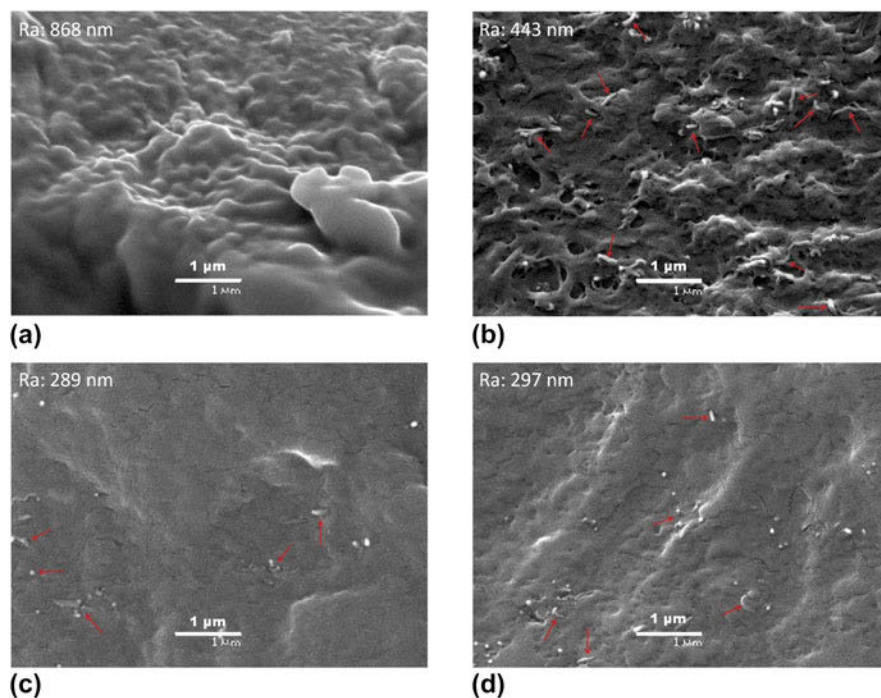
FIG. 4. SEM fracture surface images and average roughness values of (a) PHBV, (b) PHBV/P-MWCNT, (c) PHBV/MWCNT-COOH, and (d) PHBV/MWCNT-OH.

temperature (T_c) and crystallization enthalpy (ΔH_c) obtained in the cooling of neat PHBV and its nanocomposites.

In the first heating curves, it is observed that neat PHBV and its nanocomposites showed bimodal endothermic melting peaks at approximately 156 and 173 °C [Fig. 5(a)].

Double melting peaks are also observed on PHB and some other polymers. The presence of these peaks is justified by the melting of crystals with different lamellar thickness and/or different crystal structures.[29]

Liu et al.[10] studied the effect of nucleating agents on PHBV, and it was observed that either neat PHBV or its nanocomposites showed double melting temperatures in the DSC heating scan. However, for neat PHBV, the melting temperatures were lower than for the nanocomposites, indicating the worst crystal perfection with the lowest lamella thickness and confirming the effect of the nucleating agents.

It can be noted [Fig. 5(a)] that the introduction of CNTs did not affect the melting behavior and the melting temperatures on the first heating curves, as also reported by Vidhate et al.[18] and Owen et al.[30] The introduction of CNTs on plain PHBV did not significantly affect the melting enthalpies and the degree of crystallinity of PHBV but promoted its previous crystallization, as can be seen from the cooling curves [Fig. 5(b)]. In the neat PHBV, there is no crystallization peak, whereas for the nanocomposites, there is a peak at 58 ± 2 °C. This result shows that both pristine and functionalized CNTs acted as nucleating agents, promoting previous crystallization of the PHBV matrix, as mentioned before.

Xu and Qiu[1] reported that with MWCNT-COOH loadings lower than 1 wt%, there was no significant enhancement on non-isothermal melt crystallization of PHB. However, significant enhancement was obtained for loadings of 2 wt% of MWCNT-COOH.

Figure 5(c) shows the second heating curves for PHBV and its nanocomposites. Neat PHBV showed a crystallization peak at 55.5 °C. This crystallization occurs because of the increase in mobility of the PHBV chains, which allows the chains to organize and form crystallites. For the nanocomposites, this peak is not observed due to the previous crystallization of the chains during the cooling. The first melting peak was slightly shifted to higher temperatures, but the intensity was highly decreased. This happened because the crystallization conditions were different than the conditions of film production. The second melting peak was slightly shifted to lower temperatures comparing with the first heating, and the enthalpies did not show significant changes.

In Fig. 5(c), it is possible to observe the drop in the baseline for neat PHBV, which shows the glass transition temperature. This drop happens sharply within a small temperature range. For the nanocomposites, this drop in the baseline is not defined and occurs in a larger temperature range. This could be explained because the amorphous phase in the nanocomposites is smaller than
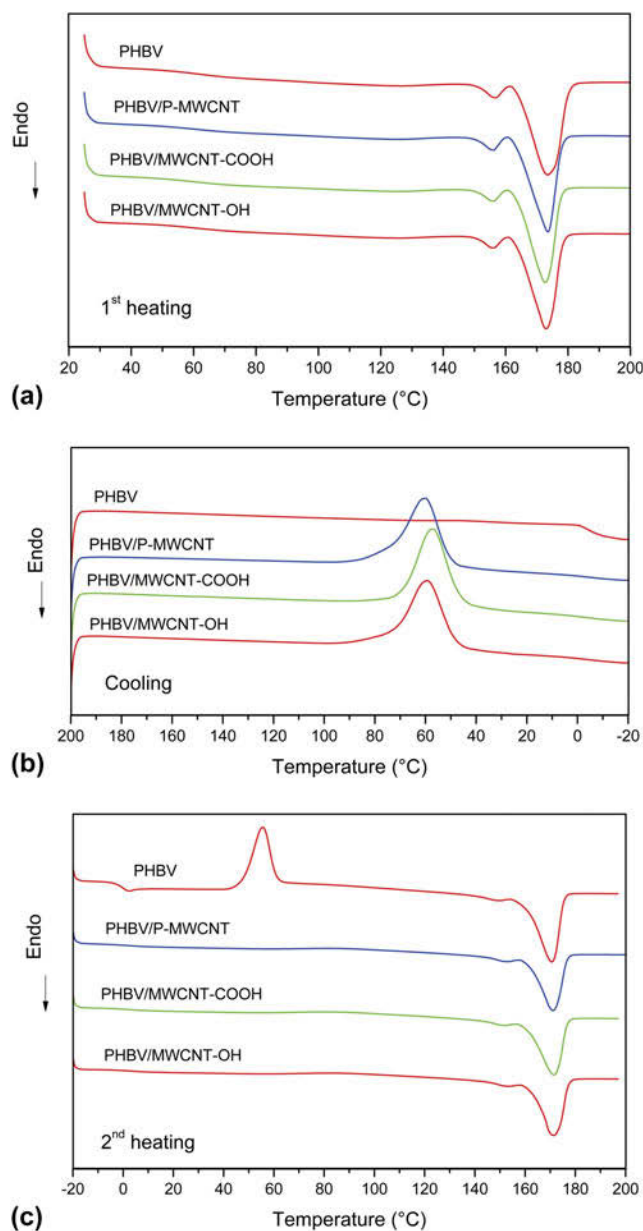
FIG. 5. DSC curves for neat PHBV and PHBV/MWCNT nanocomposites: (a) first heating, (b) cooling, and (c) second heating.

in neat PHBV, due to the previous chain crystallization. For neat PHBV, there is no crystallization peak on cooling, so the chains were completely amorphous. This change at the baseline corresponds to variations in the heat capacity (ΔC_p) due to chain mobility. So, it can be concluded that ΔC_p in nanocomposites is smaller than in plain PHBV.

D. Thermogravimetry (TGA)

Thermal degradation behaviors of neat PHBV and PHBV/MWCNT nanocomposites were examined using TGA under N_2 flow. The original thermogravimetric curves are shown in Fig. 6(a) and the first derivative

curves in Fig. 6(b). The derivative curves showed that the thermal degradation of pure PHBV proceeded by a one-step process with a maximum decomposition temperature.[31] The temperatures of 1% of weight loss, temperature of maximum weight loss rate (Tmax), and residual charge (RC) are shown in Table IV.

The temperature at maximum weight loss rate of PHBV and the nanocomposites was almost the same. This may be explained by the low content of CNTs (0.5%) on the samples, which did not affect the maximum weight loss temperature. Previous studies showed an increase of 16 °C in the temperature of maximum weight loss with an addition of 2% of MWCNTs on PHBV[31] and an increase of 9.3 °C adding 3% of MWCNT on PHBV.[32]

However, an increase in the thermal stability was observed in the weight loss initiation temperature. It observed an improvement of about 21 °C in the temperature of 1% weight loss in all nanocomposites, as shown in Table IV. It may be explained that due to the introduction of CNTs, the transport of combustion gas was hindered, and there was absorption of free radicals generated during polymer decomposition by the activated carbon surface.[31–33]

After the temperature of 1% weight loss, the degradation processes of pure PHBV and the nanocomposites occurred at similar temperatures, showing no effect of the CNTs in the thermal degradation of PHBV matrix.

The RC of nanocomposites with functionalized MWCNT reflected the amount of added CNTs, since the values were similar to the content of CNTs. For P-MWCNT, the RC was 0.87%, which is a little higher than the added amount. This may be explained due to the active surface of P-MWCNT that prevented the degradation of a certain amount of PHBV.

E. Electrical conductivity

Electrical conductivity measurements were performed to evaluate the influence of addition and functionalization of CNTs in the PHBV matrix. The values of electrical conductivity were obtained using the linear portion of I–V curves obtained from the equipment.

PHBV is an insulating polymer with an electrical conductivity of 5.1×10^{-13} S cm^{-1}, and the addition of CNTs in low contents (0.5%) make the nanocomposites conductors. The conductivity values are shown in Table V. The influence of MWCNT functionalization can be noted in the conductivity values. The conductivity values decreased for nanocomposites with functionalized CNTs. This may be explained because functionalization reactions create defects on the surface of the nanotubes, what harms the electrical transport.

For nanocomposites containing pristine CNTs, the electrical conductivity is 1.2×10^{-5} S cm^{-1}; with

TABLE III. Values of melting temperature (T_m), melting enthalpy (ΔH_m), degree of crystallinity (X_c), crystallization temperature (T_c), crystallization enthalpy (ΔH_c), and glass transition temperature (T_g) during cooling and second heating for neat PHBV and PHBV/MWCNT nanocomposites.

	First heating			
Sample	T_{m1} (°C)	ΔH_{m1} (J/g)	T_{m2} (°C)	ΔH_{m2} (J/g)
PHBV	156.4	3.2	173.5	43.8
PHBV/P-MWNTC	156.0	3.9	173.6	46.3
PHBV/MWNTC-COOH	156.0	3.6	172.9	48.7
PHBV/MWNTC-OH	156.0	3.3	173.0	45.8

	Cooling	
Sample	T_c (°C)	ΔH_c (J g^{-1})
PHBV	N/D	N/D
PHBV/P-MWNTC	59.9	48.4
PHBV/MWNTC-COOH	56.8	49.2
PHBV/MWNTC-OH	59.0	46.4

	Second heating						
Sample	T_c (°C)	ΔH_c (J g^{-1})	T_{m1} (°C)	T_{m2} (°C)	ΔH_m (J g^{-1})	T_g (°C)	X_c (%)
PHBV	55.5	39.2	148.4	170.7	51.3	0.22	47.1
PHBV/P-MWNTC	N/E	N/E	151.7	171.2	48.6	N/D	44.8
PHBV/MWNTC-COOH	N/E	N/E	150.6	171.5	52.6	N/D	48.5
PHBV/MWNTC-OH	N/E	N/E	152.1	171.4	48.8	N/D	45.0

N/E = nonexistent.
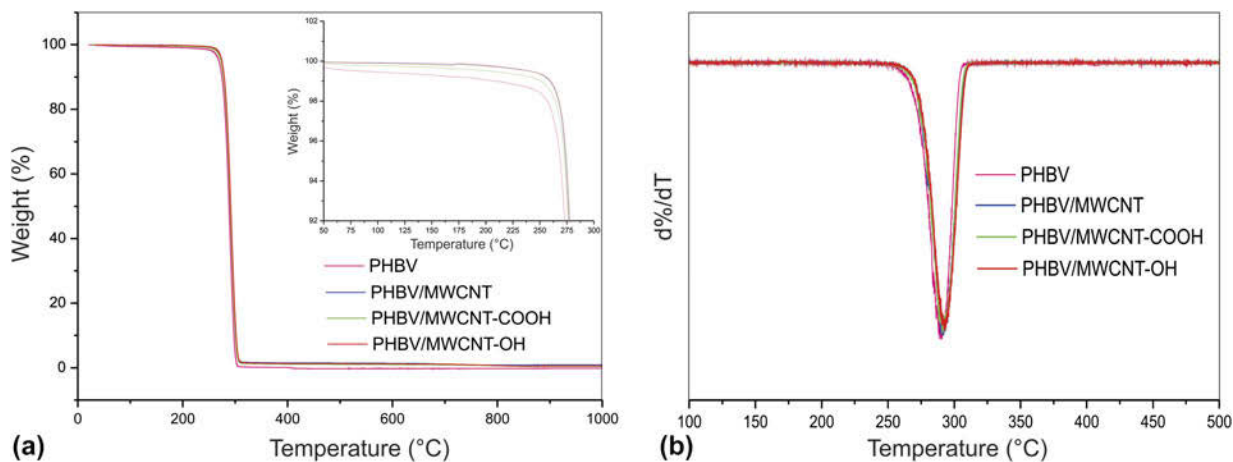N/D = not determined.

FIG. 6. Thermal degradation of neat PHBV and PHBV/MWCNT nanocomposites: (a) original thermogravimetric curves and (b) first derivative curves.

MWCNT-COOH, the conductivity decreased to 1.0×10^{-6} S cm^{-1}; and with MWCNT-OH, the value shifted to 3.0×10^{-6} S cm^{-1}.

Pristine CNTs have a perfect structure, without defects, so the charge transport is favored. With functionalization, some defects are created on the MWCNT surface, which disrupt the surface conjugation and the mode of electrical transport is modified. Carboxylic groups on the surface of oxidized CNTs (MWCNT-COOH) withdraw electrons by induction and resonance, so the charge transport is disabled. Hydroxyl groups on MWCNT surface withdraw electrons by induction, but push by resonance. That is the reason why the conductivity for nanocomposites containing reduced CNTs is higher than the ones containing MWCNT-COOH.

Some works have reported similar behaviors of electrical conductivity. Li[34] compared the conductivity values of MWCNT/PVDF and MWCNT-COOH/PVDF composites and found lower conductivity values for the nanocomposites with oxidized CNTs. This phenomenon was justified because the carboxylic groups on the MWCNT surface change the mechanism of electrical transport,

TABLE IV. Temperatures of 1% of weight loss, temperature of maximum weight loss rate (Tmax), and RC for neat PHBV and its nanocomposites.

Sample	$T1\%$	Tmax	RC (%)
PHBV	230	294	0
PHBV/P-MWCNT	259	295	0.87
PHBV/MWCNT-COOH	251	295	0.40
PHBV/MWCNT-OH	260	296	0.57

TABLE V. Electrical Conductivity values for neat PHBV and nanocomposites with pristine, oxidized and reduced MWCNT.

Sample	Conductivity (S cm^{-1})
PHBV	5.1×10^{-13}
PHBV/MWCNT	1.2×10^{-5}
PHBV/MWCNT-COOH	1.0×10^{-6}
PHBV/MWCNT-OH	3.0×10^{-6}

decreasing the tunneling currents. So, if there are carboxylic groups between MWCNTs, it becomes difficult for the electrical transport to occur, what caused a reduction in conductivity values.

Aguilar et al[35] found that agglomeration promotes MWCNT-to-MWCNT interactions through surface contact (or tunneling) and hence it increases the electrical conductivity of the composites. Overall, the authors found conductivity values of the agglomerated films larger than that of the uniformly dispersed ones, irrespective of MWCNT loading, and it was justified by the increased MWCNT-to-MWCNT contact/junctions in the agglomerated state.

V. CONCLUSION

According to the results, we can conclude that the functionalization of CNTs change the properties of MWCNTs and the properties of PHBV/MWCNT nanocomposites. The oxidation and reduction reactions improve MWCNT aqueous suspension stability, reflecting on their dispersion in the nanocomposites, as shown in the SEM images. The functionalization of MWCNT also reduces the surface roughness of the nanocomposites. Adding only 0.5 wt% of pristine and functionalized CNTs in the PHBV matrix promoted and facilitated its crystallization and increased its thermal degradation temperature, without changing the degradation behavior of the matrix. A small amount of CNTs added to PHBV makes the polymer a conductor, and functionalization harm the electrical transport, reducing conductivity values. The small shift to higher conductivity values for the nanocomposite with MWCNT-OH compared with the ones with MWCNT-COOH and P-MWCNT makes this kind of functionalization suitable to further studies for electrical applications, once that it implies in better dispersion of the tubes in the polymer matrix.

REFERENCES

1. C. Xu and Z. Qiu: Nonisothermal melt crystallization and subsequent melting behavior of biodegradable poly (hydroxybutyrate)/multiwalled carbon nanotubes nanocomposites. *J. Polym. Sci., Part B: Polym. Phys.* **47**, 2238 (2009).
2. M.M. Reddy, S. Vivekanandhan, M. Misra, S.K. Bhatia, and A.K. Mohanty: Biobased plastics and bionanocomposites: Current status and future opportunities. *Prog. Polym. Sci.* **38**, 1653 (2013).
3. C.S. Reddy, R. Ghai, and V. Kalia: Polyhydroxyalkanoates: An overview. *Bioresour. Technol.* **87**, 137 (2003).
4. L. Shang, Q. Fei, Y.H. Zhang, X.Z. Wang, D-D. Fan, and H.N. Chang: Thermal properties and biodegradability studies of Poly(3-hydroxybutyrate-co-3-hydroxyvalerate). *J. Polym. Environ.* **20**, 23 (2011).
5. E. Zribi-Maaloul, I. Trabelsi, L. Elleuch, H. Chouayekh, and R.B. Salah: Purification and characterization of two polyhydroxyalcanoates from Bacillus cereus. *Int. J. Biol. Macromol.* **61**, 82 (2013).
6. J.C. Fradinho, J.M.B. Domingos, G. Carvalho, A. Oehmen, and M.A.M. Reis: Polyhydroxyalkanoates production by a mixed photosynthetic consortium of bacteria and algae. *Bioresour. Technol.* **132**, 146 (2013).
7. J. Eggers and A. Steinbüchel: Poly(3-hydroxybutyrate) degradation in Ralstonia eutropha H16 is mediated stereoselectively to (S)-3-hydroxybutyryl coenzyme A (CoA) via crotonyl-CoA. *J. Bacteriol.* **195**, 3213 (2013).
8. A.N. Boyandin, V.P. Rudnev, V.N. Ivonin, S.V. Prudnikova, K.I. Korobikhina, M.L. Filipenko, T.G. Volova, and A.J. Sinskey: Biodegradation of polyhydroxyalkanoate films in natural environments. *Macromol. Symp.* **320**, 38 (2012).
9. W.V. Srubar, S. Pilla, Z.C. Wright, C.A. Ryan, J.P. Greene, C.W. Frank, and S.L. Billington: Mechanisms and impact of fiber–matrix compatibilization techniques on the material characterization of PHBV/oak wood flour engineered biobased composites. *Compos. Sci. Technol.* **72**, 708 (2012).
10. W.J. Liu, H.L. Yang, Z. Wang, L.S. Dong, and J.J. Liu: Effect of nucleating agents on the crystallization of poly(3-hydroxybutyrate-co-3-hydroxyvalerate). *J. Appl. Polym. Sci.* **86**, 2145 (2002).
11. M. Avella, G. Bogoeva-Gaceva, A. Buz, M.E. Errico, G. Gentile, and A. Grozdanov: Biocomposites reinforced with kenaf fibers. *J. Appl. Polym. Sci.* **104**, 3192 (2007).
12. A. El-Hadi, R. Schnabel, E. Straube, G. Müller, and S. Henning: Correlation between degree of crystallinity, morphology, glass temperature, mechanical properties and biodegradation of poly (3-hydroxyalkanoate) PHAs and their blends. *Polym. Test.* **21**, 665 (2002).
13. P.M. Ajayan: Nanotubes from carbon. *Chem. Rev.* **99**, 1787 (1999).
14. M.A. Atieh, O.Y. Bakather, B. Al-Tawbini, A.A. Bukhari, F.A. Abuilaiwi, and M.B. Fettouhi: Effect of carboxylic functional group functionalized on carbon nanotubes surface on the removal of lead from water. *Bioinorg. Chem. Appl.* **2010**, 1 (2010).
15. N.G. Sahoo, S. Rana, J.W. Cho, L. Li, and S.H. Chan: Polymer nanocomposites based on functionalized carbon nanotubes. *Prog. Polym. Sci.* **35**, 837 (2010).
16. M. Moniruzzaman and K.I. Winey: Polymer nanocomposites containing carbon nanotubes. *Macromolecules* **39**, 5194 (2006).
17. H. Hu, A. Yu, E. Kim, B. Zhao, M.E. Itkis, E. Bekyarova, and R.C. Haddon: Influence of the zeta potential on the dispersability and purification of single-walled carbon nanotubes. *J. Phys. Chem. B* **109**, 11520 (2005).
18. S. Vidhate, L. Innocentini-Mei, and N.A.D. Souza: Mechanical and electrical multifunctional poly (3-hydroxybutyrate- co -3-hydroxyvalerate)— multiwall carbon nanotube nanocomposites. *Polym. Eng. Sci.* **52**, 1367 (2012).

19. C-X. Liu and J-W. Choi: Improved dispersion of carbon nanotubes in polymers at high concentrations. *Nanomaterials* **2**, 329 (2012).

20. P.C. Ma, J-K. Kim, and B.Z. Tang: Functionalization of carbon nanotubes using a silane coupling agent. *Carbon* **44**, 3232 (2006).

21. S. Chen, W. Shen, G. Wu, D. Chen, and M. Jiang: A new approach to the functionalization of single-walled carbon nanotubes with both alkyl and carboxyl groups. *Chem. Phys. Lett.* **402**, 312 (2005).

22. L. Stobinski, B. Lesiak, L. Kövér, J. Tóth, S. Biniak, G. Trykowski, and J. Judek: Multiwall carbon nanotubes purification and oxidation by nitric acid studied by the FTIR and electron spectroscopy methods. *J. Alloys Compd.* **501**, 77 (2010).

23. B. Scheibe, E. Borowiak-Palen, and R.J. Kalenczuk: Oxidation and reduction of multiwalled carbon nanotubes - preparation and characterization. *Mater. Charact.* **61**, 185 (2010).

24. L. Liu, Y. Qin, Z. Guo, and D. Zhu: Reduction of solubilized multi-walled carbon nanotubes. *Carbon* **41**, 331 (2003).

25. C. Damian, M. Andreea, and H. Iovu: Ethylenediamine functionalization effect on the thermo-mechanical properties of epoxy nanocomposites reinforced with multiwall carbon nanotubes. *U.P. B. Sci. Bull.* **72**, 163 (2010).

26. E.F. Antunes, A.O. Lobo, E.J. Corat, V.J. Trava-Airoldi, A.A. Martin, and C. Veríssimo: Comparative study of first- and second-order Raman spectra of MWCNT at visible and infrared laser excitation. *Carbon* **44**, 2202 (2006).

27. S. Osswald, M. Havel, and Y. Gogotsi: Monitoring oxidation of multiwalled carbon nanotubes by Raman spectroscopy. *J. Raman Spectrosc.* **38**, 728 (2007).

28. M.T. Byrne, W.P. McNamee, and Y.K. Gun'ko: Chemical functionalization of carbon nanotubes for the mechanical reinforcement of polystyrene composites. *Nanotechnology* **19**, 1 (2008).

29. L.M.W.K. Gunaratne, R.A. Shanks, and G. Amarasinghe: Thermal history effects on crystallisation and melting of poly(3-hydroxybutyrate). *Thermochim. Acta* **423**, 127 (2004).

30. A.J. Owen, J. Heinzel, Ž. Škrbić, and V. Divjaković: Crystallization and melting behaviour of PHB and PHB/HV copolymer. *Polymer* **33**, 1563 (1992).

31. M. Lai, J. Li, J. Yang, J. Liu, X. Tong, and H. Cheng: The morphology and thermal properties of multi-walled carbon nanotube and poly(hydroxybutyrate-co-hydroxyvalerate) composite. *Polym. Int.* **53**, 1479 (2004).

32. H-Y. Yu, J-M. Yao, Z-Y. Qin, L. Liu, and X-G. Yang: Comparison of covalent and noncovalent interactions of carbon nanotubes on the crystallization behavior and thermal properties of poly(3-hydroxybutyrate- co -3-hydroxyvalerate). *J. Appl. Polym. Sci.* **130**, 4299 (2013).

33. M.S.P. Shaffer and A.H. Windle: Fabrication and characterization of carbon nanotube/poly(vinyl alcohol) composites. *Adv. Mater.* **11**, 937 (1999).

34. Q. Li: Temperature dependence of the electrical properties of the carbon nanotube/polymer composites. *eXPRESS Polym. Lett.* **3**, 769 (2009).

35. J.O. Aguilar, J.R. Bautista-Quijano, and F. Avilés: Influence of carbon nanotube clustering on the electrical conductivity of polymer composite films. *eXPRESS Polym. Lett.* **4**, 292 (2010).

J. Mater. Res., Vol. 30, No. 1, Jan 14, 2015

65